Обзор статей из журналов Nature и

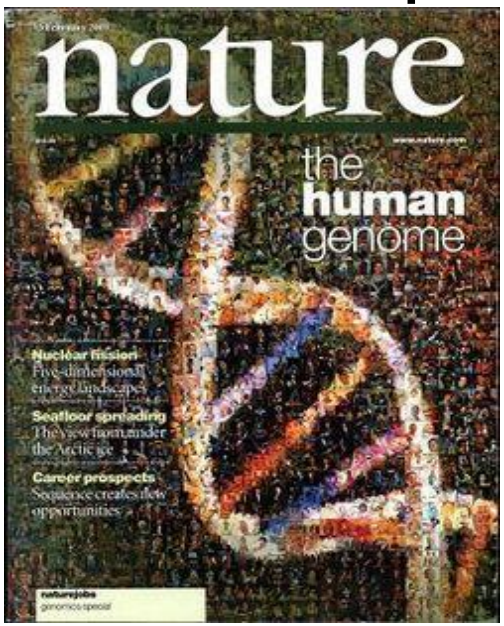

Шуман
Леонид

Правосторонний сигнальный путь приводит к формированию изгиба сердечной трубки у позвоночных

LETTER

doi:10.1038/nature23454

A right-handed signalling pathway drives heart looping in vertebrates

Oscar H. Ocaña[1], Hakan Coskun[1], Carolina Minguillón[2]†, Prayag Murawala[3]†, Elly M. Tanaka[3]†, Joan Galcerán[2], Ramón Muñoz-Chápuli[4,5] & M. Angela Nieto[1]

Most animals show external bilateral symmetry, which hinders the observation of multiple internal left–right (L/R) asymmetries that are fundamental to organ packaging and function[1,2]. In vertebrates, left identity is mediated by the left-specific Nodal–Pitx2 axis that is repressed on the right-hand side by the epithelial–mesenchymal transition (EMT) inducer Snail1 (refs 3, 4). Despite some existing evidence[3,5], it remains unclear whether an equivalent instructive pathway provides right-hand-specific information to the embryo. Here we show that, in zebrafish, BMP mediates the L/R asymmetric activation of another EMT inducer, Prrx1a, in the lateral plate mesoderm with higher levels on the right. Prrx1a drives L/R differential cell movements towards the midline, leading to a leftward displacement of the cardiac posterior pole through an actomyosin-dependent mechanism. Downregulation of Prrx1a prevents heart looping and leads to mesocardia. Two parallel and mutually repressed pathways, respectively driven by Nodal and BMP on the left and right lateral plate mesoderm, converge on the asymmetric activation of the transcription factors Pitx2 and Prrx1, which integrate left and right information to govern heart morphogenesis. This mechanism is conserved in the chicken embryo, and in the mouse SNAIL1 acts in a similar manner to Prrx1a in zebrafish and PRRX1 in the chick. Thus, a differential L/R EMT produces asymmetric cell movements and forces, more prominent from the right, that drive heart laterality in vertebrates.

Defects in L/R asymmetry occur in 1:10,000 humans[6], and the associated morbidity and mortality usually indicate congenital heart defects[6,7]. The EMT converts epithelial cells into migratory cells, and it is required in tissues and organs that are generated after profound cell movements, such as the mesoderm and the neural crest[8]. Thus, deregulation of L/R asymmetries and EMT leads to severe congenital malformations or early embryonic lethality[1,9].

After an initial disruption in L/R symmetry in the vertebrate embryo, laterality is conferred to the organizer (node) and this information is transferred to the left lateral plate mesoderm (LPM)[1]. The left-specific programme in the LPM is driven by Nodal and its downstream target Pitx2. This pathway is conserved in deuterostomes, and in chick and mouse embryos it is repressed on the right-hand side by the EMT-inducer SNAIL1 (refs 3, 4). We have found that like Snail1 in amniotes, a *prrx1* gene duplicate (*prrx1a*), is transiently expressed in the LPM of the zebrafish embryo with higher levels on the right (Fig. 1a). Prrx1, like Pitx2, is a paired-like homeobox transcription factor, and like Snail1, is an EMT inducer in embryos and cancer cells[10].

In vertebrates, the convergence of the left and right cardiogenic regions in the embryonic midline results in the formation of a linear primary heart tube (PHT). The subsequent bilateral addition of progenitor cells to the arterial (anterior) and venous (posterior) poles from the corresponding second heart fields (SHFs), respectively contribute to the elongation and growth of the heart at the outflow and inflow tracts[11]. These additions occur at the time of heart looping, for which the underlying mechanisms remain poorly understood[11], although defects in the posterior pole are responsible for numerous congenital heart defects in humans. Considering Prrx1a L/R asymmetric expression and its described role in the induction of cell movements[10], we examined whether *prrx1a* knockdown influenced heart position. Both *prrx1a* morpholino oligonucleotide (*prrx1a*^{MO1} or *prrx1a*^{MO2})[10] injections or CRISPR–Cas9-driven *prrx1a* mutations led to mesocardia, a straight heart that failed to undergo the normal dextral looping (Fig. 1b, c and Extended Data Fig. 1). Both atrial and ventricular chambers are specified in the morphants (Fig. 1d), but, in addition to defective looping, the heart presented a smaller atrium and a defective posterior pole lacking a defined sinus venosus and the expression of its marker Islet1 (refs 12, 13) (Fig. 1e and Extended Data Fig. 2a–c). However, the anterior pole was not overtly affected (Extended Data Fig. 2d).

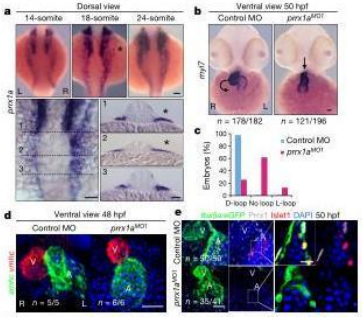

Figure 1 | *prrx1a* L/R asymmetric expression in zebrafish. a, Whole-mount *in situ* hybridization and transverse sections at the levels of the dotted lines in 14-, 18- and 24-somite stage zebrafish embryos. **b**, Heart location in control and *prrx1a*-morphant (*prrx1a*^{MO1}) embryos analysed for the cardiomyocyte marker *myl7*. hpf, hours post fertilization; MO, morpholino. **c**, Quantification of heart location. **d**, Analysis of atrial (A) and ventricular (V) markers *amhc* (also known as *myh6*) and *vmhc*, respectively. **e**, Confocal analysis of Prrx1 and Islet1 expression in transgenic zebrafish embryos *Tg(tbx5a:eGFP)*. Nuclei were stained with DAPI. Asterisks indicate areas of asymmetry. Scale bars, 50 μm or 10 μm (enlarged images in **e**).

В работе коллектива испанских и германских учёных исследуются молекулярные механизмы формирования право-левосторонней ассиметрии у позвоночных животных .

Конкретно, изучается влияние фактора BMP и опосредуемого им Prrx1 на правосторонне смещение зачатка сердечной мышцы у эмбрионов.

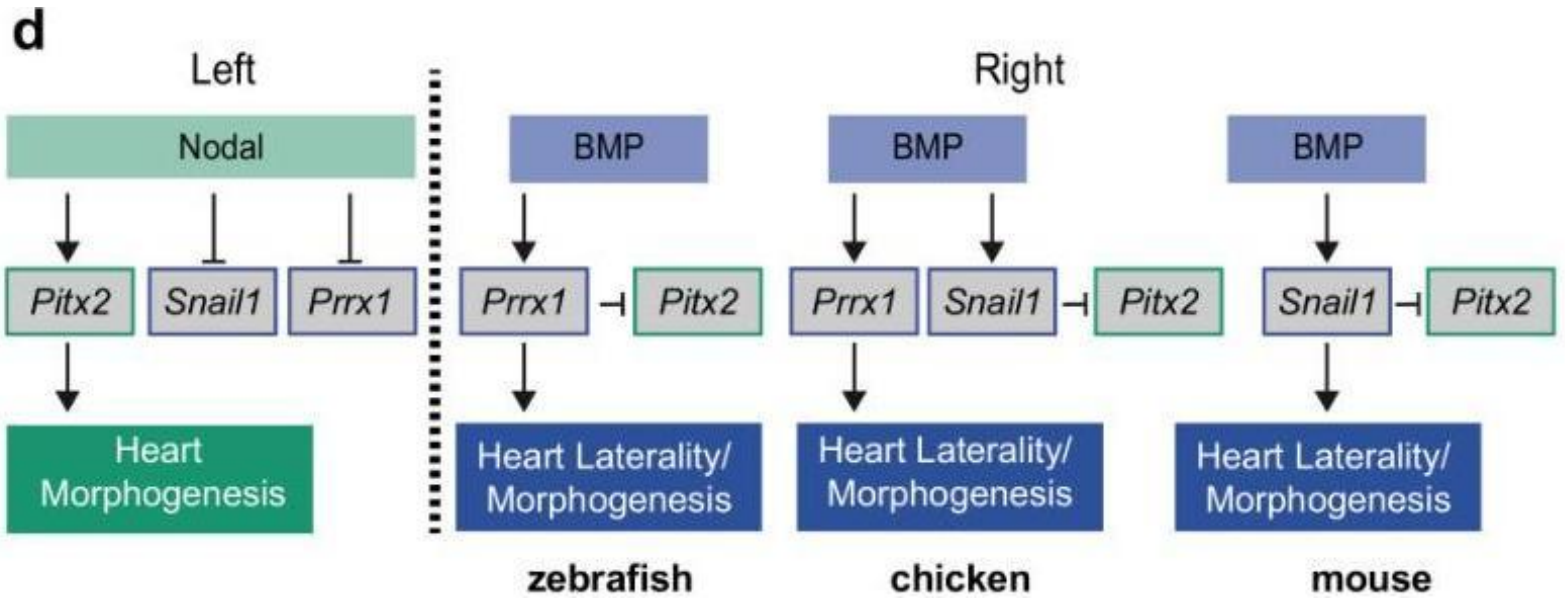
d
Left
Right
Nodal
BMP
BMP
BMP
Pitx2
Snail1
Prrx1
Prrx1
Pitx2
Prrx1
Snail1
Pitx2
Snail1
Pitx2
Heart Morphogenesis
Heart Laterality/ Morphogenesis
Heart Laterality/ Morphogenesis
Heart Laterality/ Morphogenesis
zebrafish
chicken
mouse

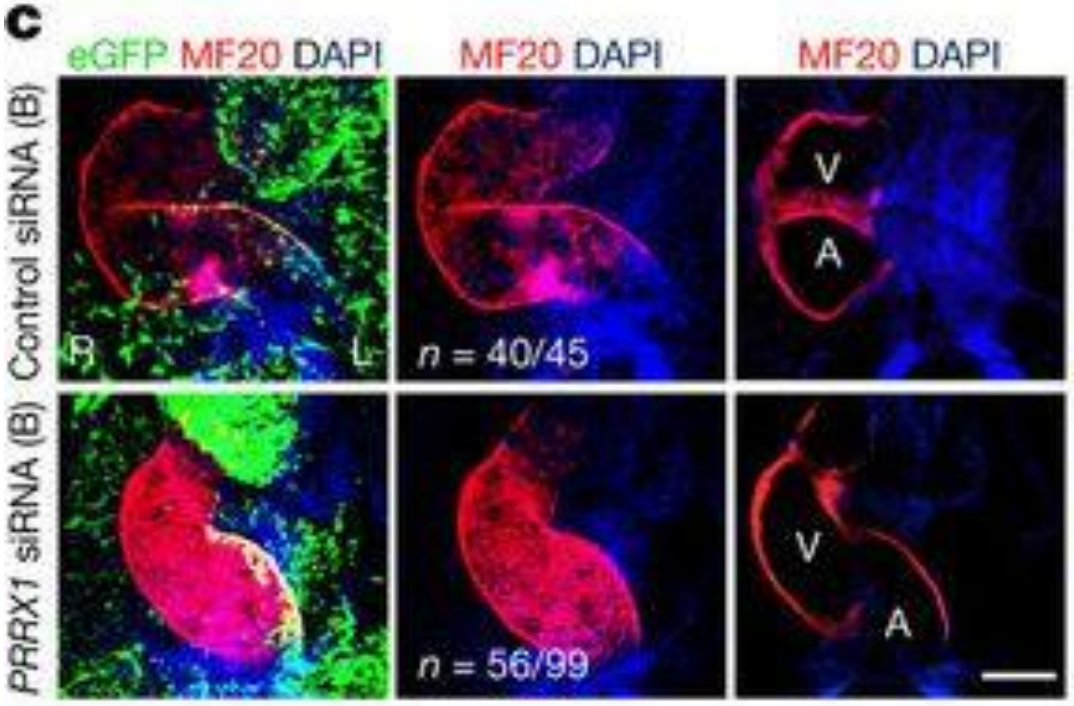
c
eGFP MF20 DAPI
MF20 DAPI
MF20 DAPI
Control siRNA (B)
PRRX1 siRNA (B)
R
L
n = 40/45
n = 56/99
V
A
V
A

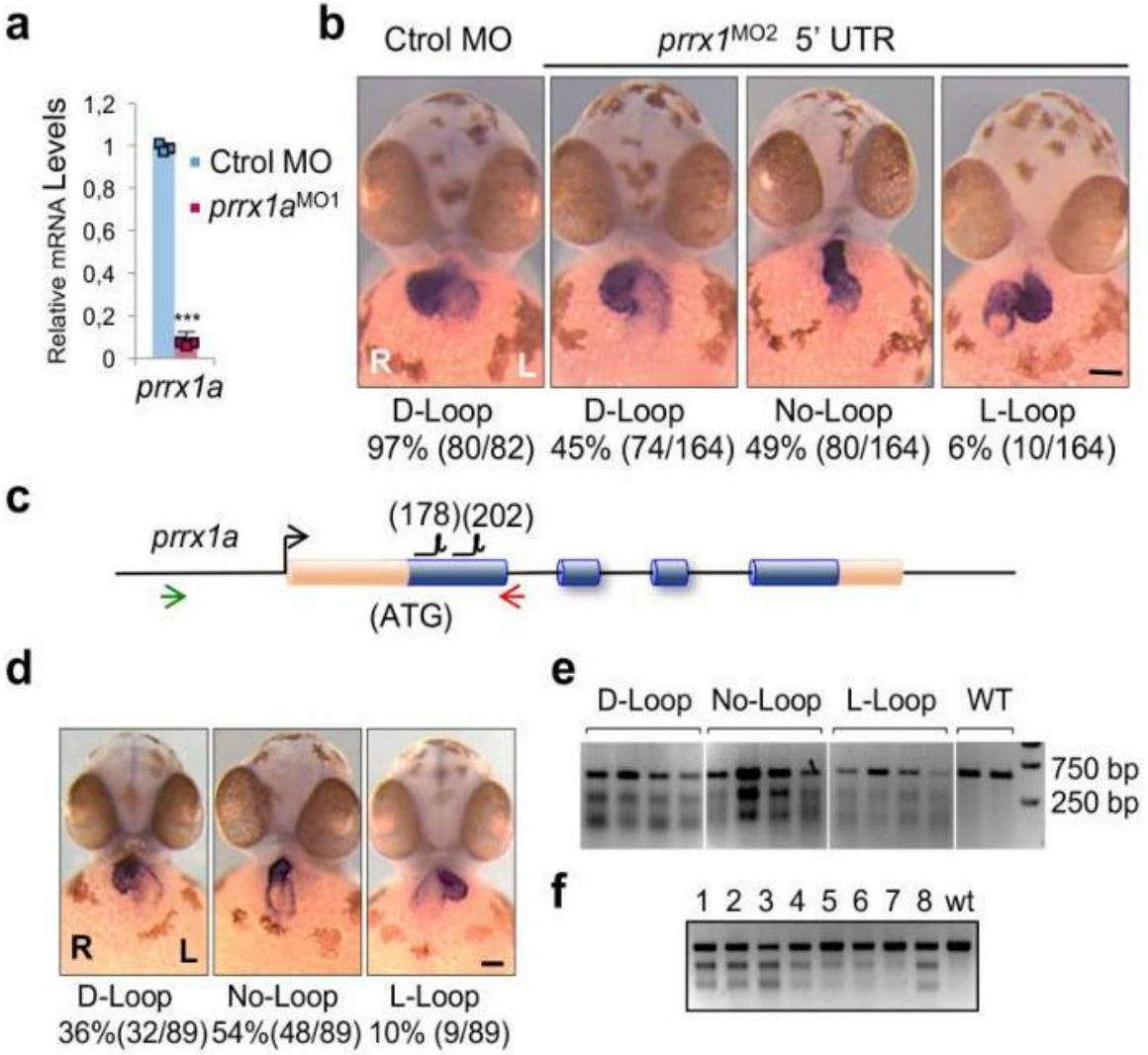
a
Relative mRNA Levels
1,2
1
0,8
0,6
0,4
0,2
0
Ctrol MO
prrx1aMO1
***
prrx1a
b
Ctrol MO
prrx1MO2 5' UTR
R
L
D-Loop
97% (80/82)
D-Loop
45% (74/164)
No-Loop
49% (80/164)
L-Loop
6% (10/164)
c
prrx1a
(178)(202)
(ATG)
d
R
L
D-Loop
36%(32/89)
No-Loop
54%(48/89)
L-Loop
10% (9/89)
e
D-Loop
No-Loop
L-Loop
WT
750 bp
250 bp
f
1 2 3 4 5 6 7 8 wt
g
TCATGACTTCCAGCTATGCTCATGTAATGGACAGACAAGCCACACTACCAAACCGACTGGAGACTGCGATCACCGCGAATCAGGATCATTTACAGGCT Emb
TCATGACTTCCAGCTATGCTCATGTAATGGACAGACAAGCCACACTACCAAACCGACTGGAGACTGCGATCACCG-----CAGGATCATTTACAGGCT 1
TCATGACTTCCAGCTATGCTCATGTAATGGACAGACAAGCCACACTACCAAACCGACTGGAGACTGCGATCACCGCGA-TCAGGATCATTTACAGGCT 1
----------CCACACATGCTAACGTAATGGAGACTGCGATCACCGCGAATCAGGATCATTTACAGGCT 2
TCATGACTTCCAGCTATGCTCATGTAATGGACAGACAAGCCACACTACCAAACCGACTGGAGACTGCGATCACCGCGA-------TCATTTACAGGCT 2
TCATGACTTCCATCTATGCTCATGTAATGGGCGCACAAGCCACACTACCAAACCGACTGGAGACTGCGATCACCGCGAATCAGGATCATTTACAGGCT 5
TCATGACTTCCAGCTATGCTCATGTAATGGACAGACAAGCCACACTACCAA----ACTGGAGACTGCGATCACCGCGAATCAGGATCATTTACAGGCT 5
TCATGACTTCCAGCTATGCTCATGTAATGGACAGACAAGCCACACTACCAAACCGACTGGAGACTGCGATCA----------GGATCATTTACAGGCT 5

Как CRISPR-Cas типа II устанавливает иммунитет с помощью интеграции спейсеров опосредованной Cas1-Cas2

LETTER

doi:10.1038/nature24020

How type II CRISPR–Cas establish immunity through Cas1–Cas2–mediated spacer integration

Yibei Xiao[1], Sherwin Ng[1]*, Ki Hyun Nam[2]* & Ailong Ke[1]

CRISPR (clustered regularly interspaced short palindromic repeats) and the nearby *cas* (CRISPR-associated) operon establish an RNA-based adaptive immunity system in prokaryotes[1–5]. Molecular memory is created when a short foreign DNA-derived prespacer is integrated into the CRISPR array as a new spacer[6–9]. Whereas the RNA-guided CRISPR interference mechanism varies widely among CRISPR-Cas systems, the spacer integration mechanism is essentially identical[7–9]. The conserved Cas1 and Cas2 proteins form an integrase complex consisting two distal Cas1 dimers bridged by a Cas2 dimer in the middle[6,10]. The prespacer is bound by Cas1-Cas2 as a dual forked DNA, and the terminal 3′-OH of each 3′-overhang serves as an attacking nucleophile during integration[11–13]. Importantly, the prespacer is preferentially integrated into the leader-proximal region of the CRISPR array[1,7,10,15], guided by the leader sequence and a pair of inverted repeats (IRs) inside the CRISPR repeat[7,15–20]. Spacer integration in the most well-studied *Escherichia coli* Type I-E CRISPR system further relies on the bacterial Integration Host Factor (IHF)[21,22]. In Type II-A CRISPR, however, Cas1-Cas2 alone integrates spacer efficiently *in vitro*[18]; other Cas proteins (Cas9 and Csn2) play accessory roles in prespacer biogenesis[17,23]. Focusing on the *Enterococcus faecalis* Type II-A system[24], here we report four structure snapshots of Cas1-Cas2 during spacer integration. *Efa*Cas1-Cas2 selectively binds to a splayed 30-bp prespacer bearing 4-nt 3′-overhangs. Three molecular events take place upon encountering a target: Cas1-Cas2/prespacer first searches for half-sites stochastically, then preferentially interacts with the leader-side CRISPR repeat and catalyzes a nucleophilic attack that connects one strand of the leader-proximal repeat to the prespacer 3′-overhang. Recognition of the spacer half-site requires DNA bending and leads to full integration. We derive a mechanistic framework explaining the stepwise spacer integration process and the leader-proximal preference.

*Efa*Cas1-Cas2 preferred a splayed prespacer containing a 22-bp mid-duplex and two 4-nt 3′-overhangs (Fig. 1a-b). The leader half-site is preferred; integration reached completion within seconds, whereas the spacer-side integration took minutes and plateaued to a lesser extent (Fig. 1c). The first 4-bp of the leader was sufficient in guiding the leader-side integration; trimming sequences further upstream had negligible effect (Fig. 1d). Complementing the spacer-side IR sequence selectively abolished spacer-side integration, whereas the same change in leader-side IR still allowed some integration to the leader-side (Fig. 1d). These observations suggest that the leader and IR work synergistically to guide the leader-side integration, whereas the spacer-side integration relies primarily on the spacer-side IR. Based on the biochemistry, we designed the splayed prespacer and minimum leader-repeat substrates for crystallization and determined the *Efa*Cas1-2/prespacer binary structure and two *Efa*Cas1-2/prespacer/target ternary structures (Extended Data Tables 1–2).

Whereas *E. coli* Cas1-Cas2 integrates a 33-bp prespacer into the beginning and end of a 28-bp CRISPR repeat, *E. fae* Cas1-Cas2 prefers a shorter prespacer (30-bp), but a longer repeat (36-bp). Comparison of the two Cas1-Cas2/prespacer structures nicely explain their distinct substrate preferences (Fig. 2)[11,12]. Both adopt a dumbbell-shaped architecture, in which two asymmetrically assembled Cas1 dimers are handcuffed by a Cas2 dimer in the middle (Fig. 2a). Only one Cas1 in each dimer catalyzes spacer integration; the other is oriented incorrectly. In comparison to the *E. coli* counterpart, *Efa*Cas2 dimerizes at a tilted angle rather than in a juxtaposed fashion; the dimer orients in parallel rather than in perpendicular to the axis of the prespacer; and the Cas1-Cas2 contact is mediated by the C-terminal tail from the adjacent Cas2, rather than from the domain-swapped Cas2 (Fig. 2a; Extended Data Figures 1–3). These factors contribute to a ~15 Å extension between the two Cas1 active sites, allowing *Efa*Cas1-Cas2 to integrate prespacers into an 8-bp longer repeat. *Efa*Cas1-Cas2 further displays two positively-charged stripes and chelates two Mg^{2+} ions to mediate favorable contacts to prespacer backbone (Fig. 2b-e). Consistent with biochemistry, *Efa*Cas1-Cas2 displays the 30-bp prespacer as a 22-bp duplex with a 4-bp splayed region at each end. The duplex length is specified by the end-stacking of His11 in each catalytic Cas1 (Fig. 2c). The two overhangs are guided to different paths by the positive charges in Cas1: 5′-overhang to Cas1-NTD and 3′-overhang to Cas1-CTD (Fig. 2f). Interestingly, the 3′-overhang is not stably docked in the active site and has equal propensity to fold into a tetraloop (Fig. 2f).

To understand the spacer integration mechanism, we determined a 3.1 Å *Efa*Cas1-Cas2/prespacer/target ternary structure. The target contains a CRISPR repeat flanked by two 5-bp leaders to promote full-integration. To our surprise, the structure instead captures two Cas1-Cas2/prespacer complexes bound to one target; one Cas1-Cas2 is sampling dsDNA nonspecifically, and the other is catalyzing the leader-side half-integration (Fig. 3a). The sequence-nonspecific DNA contacts are similar in these two states. Each Cas2 contributes Thr78 and a nearby positive patch (K80/Q81/R84) to form a fulcrum to balance the target in the middle, ~30 Å above the prespacer and with a ~30° included angle (Fig. 3b-d). Because Cas1 active sites are recessive relative to the Cas2 fulcrum, the two half-sites cannot simultaneously access the active sites without a bend in the middle, therefore half-site recognition must take place in a sequential fashion. Lacking sequence-specific contacts, the target DNA in the substrate-sampling structure still dips down towards the Cas1 active site at one end and tips up at the other (Fig. 3c). This is because each non-catalytic Cas1 contacts target with a Lys-rich β-hairpin (K-finger: K255/K256/K257/Q258), and one K-finger contact is 3-bp closer to the fulcrum than the other, resulting in DNA tilting (Fig. 3e).

The half-integration snapshot provides direct evidence that the two integration events happen in a sequential fashion. A more pronounced DNA tilting enables the catalytic Cas1 subunit to gain direct contact, inserting an α-helix (aa145-159; hence named the leader-recognition helix) into the minor groove of the leader duplex (Fig. 4a-b; Extended Data Figure 4). Normally DNA minor groove is too narrow

[1]Department of Molecular Biology and Genetics, Cornell University, 253 Biotechnology Building, Ithaca, New York 14853, USA. [2]Pohang Accelerator Laboratory, Pohang University of Science and Technology, Pohang, South Korea.
*These authors contributed equally to this work.

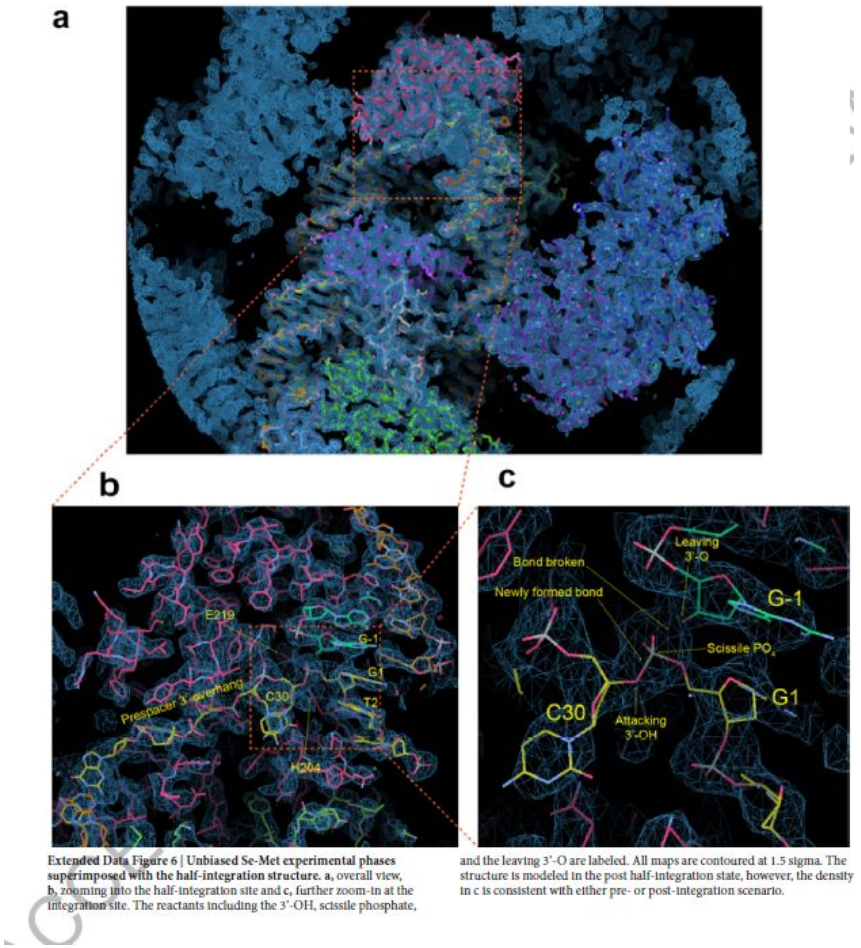

Extended Data Figure 6 | Unbiased Se-Met experimental phases superimposed with the half-integration structure. a, overall view, **b,** zooming into the half-integration site and **c,** further zoom-in at the integration site. The reactants including the 3′-OH, scissile phosphate, and the leaving 3′-O are labeled. All maps are contoured at 1.5 sigma. The structure is modeled in the post half-integration state, however, the density in c is consistent with either pre- or post-integration scenario.

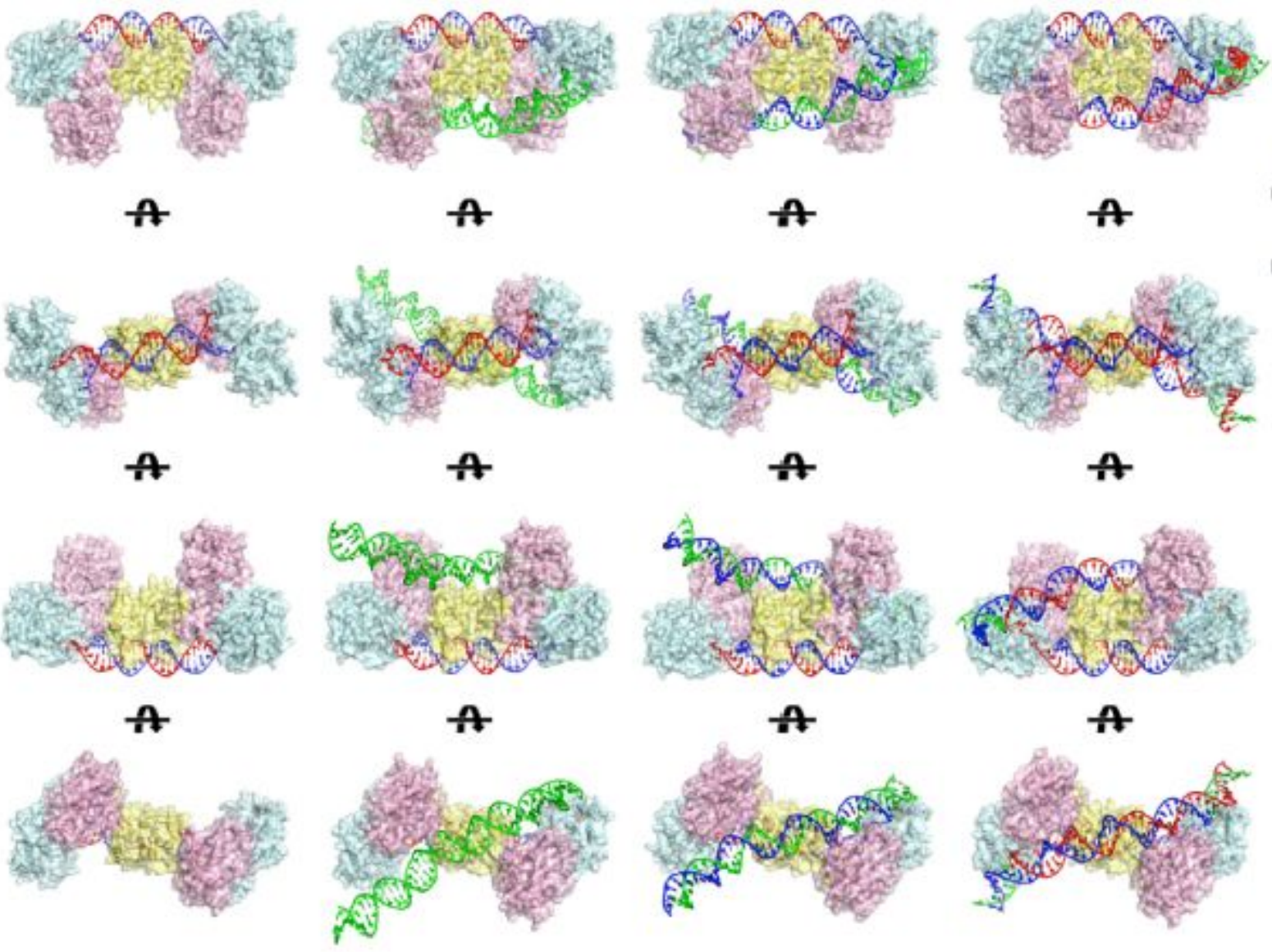

Extended Data Figure 1 | Comparison of *Efa*Cas1-Cas2 structures in prespacer-bound, target-sampling, half-integration, and full-integration states.

m^{6}A модулирует специализацию гемопоэтических стволовых клеток и клеток-предшественников

LETTER

doi:10.1038/nature23883

m^{6}A modulates haematopoietic stem and progenitor cell specification

Chunxia Zhang[1,2]*, Yusheng Chen[2,3]*, Baofa Sun[3]*, Lu Wang[1]*, Ying Yang[3]*, Dongyuan Ma[1], Junhua Lv[1,2], Jian Heng[1,2], Yanyan Ding[1,2], Yuanyuan Xue[1,2], Xinyan Lu[1,2], Wen Xiao[3], Yun-Gui Yang[2,3] & Feng Liu[1,2]

N^6-methyladenosine (m^{6}A) has been identified as the most abundant modification on eukaryote messenger RNA (mRNA)[1]. Although the rapid development of high-throughput sequencing technologies has enabled insight into the biological functions of m^{6}A modification[2–13], the function of m^{6}A during vertebrate embryogenesis remains poorly understood. Here we show that m^{6}A determines cell fate during the endothelial-to-haematopoietic transition (EHT) to specify the earliest haematopoietic stem/progenitor cells (HSPCs) during zebrafish embryogenesis. m^{6}A-specific methylated RNA immunoprecipitation combined with high-throughput sequencing (MeRIP–seq) and m^{6}A individual-nucleotide-resolution cross-linking and immunoprecipitation with sequencing (miCLIP–seq) analyses reveal conserved features on zebrafish m^{6}A methylome and preferential distribution of m^{6}A peaks near the stop codon with a consensus RRACH motif. In *mettl3*-deficient embryos, levels of m^{6}A are significantly decreased and emergence of HSPCs is blocked. Mechanistically, we identify that the delayed YTHDF2-mediated mRNA decay of the arterial endothelial genes *notch1a* and *rhoca* contributes to this deleterious effect. The continuous activation of Notch signalling in arterial endothelial cells of *mettl3*-deficient embryos blocks EHT, thereby repressing the generation of the earliest HSPCs. Furthermore, knockdown of *Mettl3* in mice confers a similar phenotype. Collectively, our findings demonstrate the critical function of m^{6}A modification in the fate determination of HSPCs during vertebrate embryogenesis.

In vertebrates, HSPCs are derived from haemogenic endothelium, a subset of endothelial cells in the ventral wall of dorsal aorta, through endothelial-to-haematopoietic transition[14–16] during embryogenesis. Previous studies have suggested the role of m^{6}A modification in cell fate determination and lineage transition in embryonic stem cells[17–19]. However, the exact physiological function of m^{6}A modification in vertebrate definitive haematopoiesis remains unknown. Given the early lethality of mice with knockout of m^{6}A methyltransferase catalytic subunit *Mettl3*[19], here we investigate the m^{6}A methylome during embryogenesis using zebrafish. Our previous studies demonstrate maternal and persistent expression of *mettl3* across different developmental stages[20], indicating the presence of m^{6}A modification during embryogenesis. Using ultra-high-performance liquid chromatography-triple quadrupole mass spectrometry, coupled with multiple-reaction monitoring (UHPLC-MRM-MS/MS) analysis, we detected high m^{6}A mRNA methylation in embryos, from 5 to 28 hours post fertilization (hpf) (Extended Data Fig. 1a).

Using MeRIP–seq[21], we profiled mRNA m^{6}A methylation in zebrafish embryos at 28 hpf, when the earliest HSPCs begin to emerge. High overlapping m^{6}A peaks were detected in two independent replicates (Extended Data Fig. 1b). Although detected in 336 non-coding RNAs (ncRNAs; 3.5%) (Extended Data Fig. 1c, d), m^{6}A mostly occurred in mRNAs (96.5%) that are involved in transcription, cell cycle, and organism development (Extended Data Fig. 1e). Around 8.4% methylated mRNAs are found to contain at least four peaks (Extended Data Fig. 1f), higher than that reported in mice (5.5%)[21]. Consistent with previous mammalian studies[21,22], m^{6}A peaks in zebrafish are significantly enriched in RGACH motif (R=G/A; H=A/C/U) (Fig. 1a), and are abundant in coding sequences (CDSs), 3′ untranslated regions (UTRs), and near stop codons (Fig. 1b, c).

To investigate the biological relevance of m^{6}A modification in embryogenesis, we used a *mettl3* morpholino (MO)[20], which caused a decrease in METTL3 protein levels (Extended Data Fig. 2a), and m^{6}A levels were significantly decreased in *mettl3* morphants (Extended Data Fig. 2b). Compared to the control embryos, there are fewer m^{6}A peaks across the entire gene bodies in *mettl3* morphants (Fig. 1c). 4,593 genes with significantly-decreased m^{6}A levels in *mettl3* morphants were identified as potential METTL3 targets (Fig. 1d), and embryonic development terms were significantly enriched in these targets

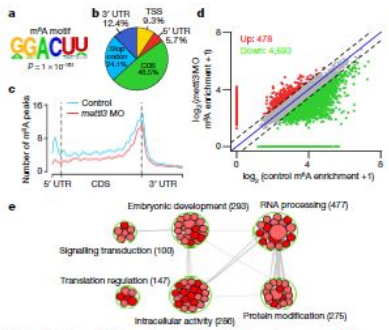

Figure 1 | m^{6}A methylome in zebrafish embryos. a, Sequence motif identified within m^{6}A peaks by HOMER database. **b**, Pie chart depicting the fraction of m^{6}A peaks in five transcript segments. **c**, Metagene profiles of m^{6}A peak distribution along a normalized transcript composed of three rescaled non-overlapping segments: 5′UTR, CDS, and 3′UTR in control and *mettl3* morphants. **d**, Scatter plots showing the m^{6}A enrichment in mRNAs of control and *mettl3* morphants. m^{6}A-containing mRNAs with significantly increased and decreased peak enrichment are highlighted in red and green, respectively (chi-square test, $P < 0.05$). **e**, Gene ontology enrichment map of METTL3 target genes.

[1]State Key Laboratory of Membrane Biology, Institute of Zoology, Chinese Academy of Sciences, Beijing 100101, China. [2]University of Chinese Academy of Sciences, Beijing 100049, China. [3]CAS Key Laboratory of Genomic and Precision Medicine, Collaborative Innovation Center of Genetics and Development, CAS Center for Excellence in Molecular Cell Science, College of Future Technology, Beijing Institute of Genomics, Chinese Academy of Sciences, Beijing 100101, China.
*These authors contributed equally to this work.

Группа исследователей из Китая изучают роль метилирования аденозина по шестой позиции в мРНК в формировании стволовых клеток крови у рыбок *Danio rerio.*

С использованием методов имуннохимического мечения метиладенозина и высокопроизводительного секвенирования РНК с детекцией метилированных аденозинов удалось показать роль этого процесса в эндотелиально-гемопоэтичеком переходе.

Эндотелиально-гемопоэтическая трансдукция (EHT) нарушается при снятии метилирования

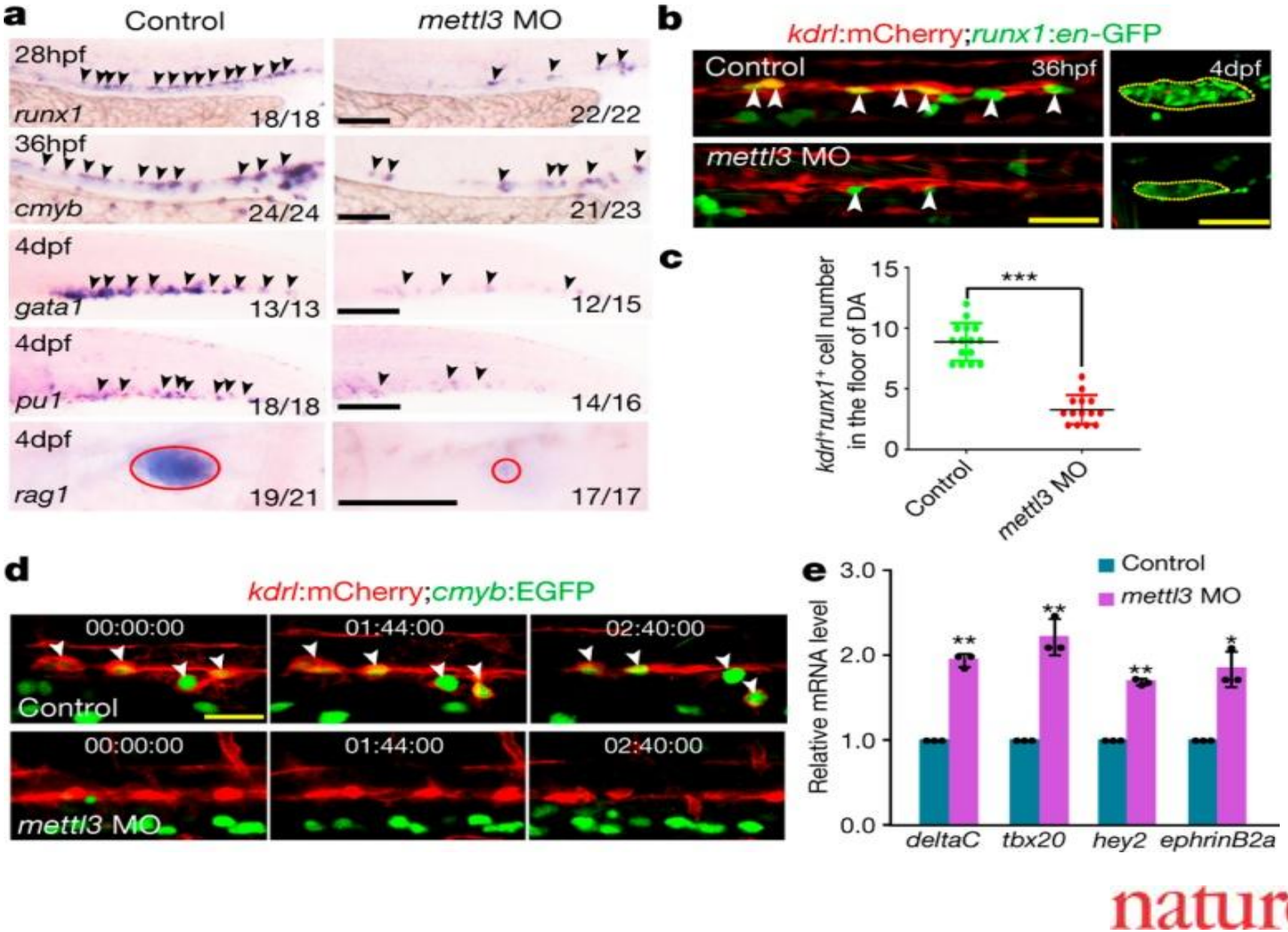

nature

Конкурирующая клеточная память митогенов и сигналов стресса p53 контролирует клеточный цикл

LETTER doi:10.1038/

Competing memories of mitogen and p53 signalling control cell-cycle entry

Hee Won Yang[1], Mingyu Chung[1], Takamasa Kudo[1] & Tobias Meyer[1]

Regulation of cell proliferation is necessary for immune responses, tissue repair, and upkeep of organ function to maintain human health[1]. When proliferating cells complete mitosis, a fraction of newly born daughter cells immediately enter the next cell cycle, while the remaining cells in the same population exit to a transient or persistent quiescent state[2]. Whether this choice between two cell-cycle pathways is due to natural variability in mitogen signalling or other underlying causes is unknown. Here we show that human cells make this fundamental cell-cycle entry or exit decision based on competing memories of variable mitogen and stress signals. Rather than erasing their signalling history at cell-cycle checkpoints before mitosis, mother cells transmit DNA damage-induced p53 protein and mitogen-induced cyclin D1 (*CCND1*) mRNA to newly born daughter cells. After mitosis, the transferred *CCND1* mRNA and p53 protein induce variable expression of cyclin D1 and the CDK inhibitor p21 that almost exclusively determines cell-cycle commitment in daughter cells. We find that stoichiometric inhibition of cyclin D1–CDK4 activity by p21 controls the retinoblastoma (Rb) and E2F transcription program in an ultrasensitive manner. Thus, daughter cells control the proliferation–quiescence decision by converting the memories of variable mitogen and stress signals into a competition between cyclin D1 and p21 expression. We propose a cell-cycle control principle based on natural variation, memory and competition that maximizes the health of growing cell populations.

We investigated how cells decide between different cell-cycle paths by using a stably transduced live-cell reporter of CDK2 activity in non-transformed human mammary epithelial MCF10A cells[2]. After mitosis, newly born daughter cells either increase CDK2 activity for continued proliferation ($CDK2^{inc}$), or decrease CDK2 activity, entering a persistent ($CDK2^{low}$) or transient ($CDK2^{delay}$) quiescent state (G0) (Fig. 1a). Selection of the CDK2 path is regulated by mitogen/RAS/MEK/ERK signalling in mother cells[2,3], activation of the cyclin D–CDK4 complex[4], and induction of E2F transcription factors[5] (Fig. 1b). Here, we explore whether and how natural variability in signalling regulates the selection of different CDK2 paths.

To determine when different steps in the mitogen signalling pathway are needed for daughter cells to enter the next cell cycle, we tested three points in the pathway by either removing mitogens or applying inhibitors of MEK (PD0325901) or CDK4 (palbociclib) in asynchronously cycling cells. When aligning cells *in silico* by the time of pathway inhibition relative to the end of mitosis, we confirmed that mitogens and MEK had to be inhibited in mother cells to effectively suppress cell-cycle entry in daughter cells[2,3] (Fig. 1c, d). By contrast, inhibition of CDK4 suppressed cell-cycle entry until 2.5 h after mitosis (Fig. 1d). By transiently removing mitogens for 5 h, we further found that a transient loss in mitogen signalling during G2 or G0/G1 phases suppressed the $CDK2^{inc}$ or $CDK2^{delay}$ paths, respectively (Extended Data Fig. 1). Taken together, these data suggest that a mediator connects mitogen/MEK/ERK to CDK4 both across mitosis to regulate $CDK2^{inc}$ cells and during G0 of daughter cells to regulate $CDK2^{delay}$ cells.

To test whether variable ERK activity in G2 directs daughter cells to the $CDK2^{inc}$ or $CDK2^{low}$ path, we established MCF10A cells stably expressing ERK[6] and CDK2 reporters (Supplementary Video 1). Control experiments confirmed that the signal measured by the ERK reporter reflects ERK activity throughout the cell cycle, except for a peak at the onset of mitosis that is not sensitive to MEK inhibition[7] (Extended Data Fig. 2). We also note that inhibition of a peak of ERK activity after mitosis did not prevent cell-cycle entry for most $CDK2^{inc}$ cells (Extended Data Fig. 3a). When we classified and averaged ERK activity based on the CDK2 paths of daughter cells, ERK activity during the G2 phase of mother cells was indeed higher in $CDK2^{inc}$ cells than in $CDK2^{delay}$ or $CDK2^{low}$ cells (Fig. 1e and Extended Data Fig. 3b, c). A calibration in Extended Data Fig. 2e showed that the mean ERK signal difference in G2 between $CDK2^{inc}$ and $CDK2^{low}$ cells corresponded to a 1.4-fold difference in levels of cyclin D1 (Fig. 1f for G2 and Extended Data Fig. 3d for G0/G1). Together with the delay between MEK and CDK4 requirement (Fig. 1d), these data suggest that naturally higher ERK signalling in mother cells may increase cyclin D–CDK4 activity in daughters to promote the $CDK2^{inc}$ path. However, when we tested how ERK activity in G2 predicts the CDK2 paths of daughter cells using an odds ratio analysis, we found that ERK activity is only partially predictive for the CDK2 path selection (Fig. 1g, left). As a reference, a blue line depicts an accurate prediction of the bifurcation in CDK2 activity (Extended Data Fig. 3e, see Methods). The partial prediction is probably not a result of noise, since odds ratios were higher for lower concentrations of mitogen stimuli (Fig. 1g, right and Extended Data Fig. 3f) or times closer to mitosis (Extended Data Fig. 3g). Thus, additional variables probably regulate CDK2 path selection.

We considered whether such an additional regulatory mechanism might be the DNA damage/p53 signalling pathway[8,9], since DNA damage is known to occur naturally during DNA replication[10] and high levels of p53-regulated p21 are correlated with cells exiting the cell cycle[2]. To determine whether p53 and p21 signals in mother cells are correlated with the CDK2 paths of daughter cells, we used live-cell analysis of MCF7 cells that had p53 and p21 tagged with different fluorescent proteins at their endogenous loci[11]. Although MCF7 is a breast cancer cell line, it has intact CDK4-dependent cell-cycle regulation[12]. Notably, when we averaged time courses of p53 and p21 expression based on the CDK2 paths of daughter cells, both protein expression levels were higher before mitosis in cells on the $CDK2^{low}$ and $CDK2^{delay}$ paths compared to the $CDK2^{inc}$ path (Fig. 2a, b and Extended Data Fig. 4a). This suggests that p53 signalling in mother cells, along with ERK signalling, is contributing to the cell-cycle decision by daughter cells.

We next tested in MCF10A cells whether p53 has a causal role in CDK2 path selection by knockout and short interfering RNA (siRNA) knockdown of p53, and observed an increase in the number of daughter cells taking the $CDK2^{inc}$ path (Extended Data Fig. 4b, c). Conversely, direct activation of p53 signalling in mother cells by transient incubation with nutlin-3 or tenovin-6 for 1 h triggered a marked reduction in the $CDK2^{inc}$ path in daughter cells (Fig. 2c and Extended Data Fig. 4d).

[1]Department of Chemical & Systems Biology, Stanford University School of Medicine, Stanford, California 94305, USA.

Группа американских учёных с азиатскими именами исследует причины ассиметричного деления клеток, когда одна из дочерних клеток продолжает деление а другая входит в состояние покоя.

Измеряя соотношение концентраций двух факторов: мРНК циклина D1 – белка индуцирующего митоз (митогена) и стрессового белка P51, исследователи научились предсказывать судьбу клетки.

DNA damage and p53 signalling in mother cells controls the CDK2^{inc} path selection in daughter cells

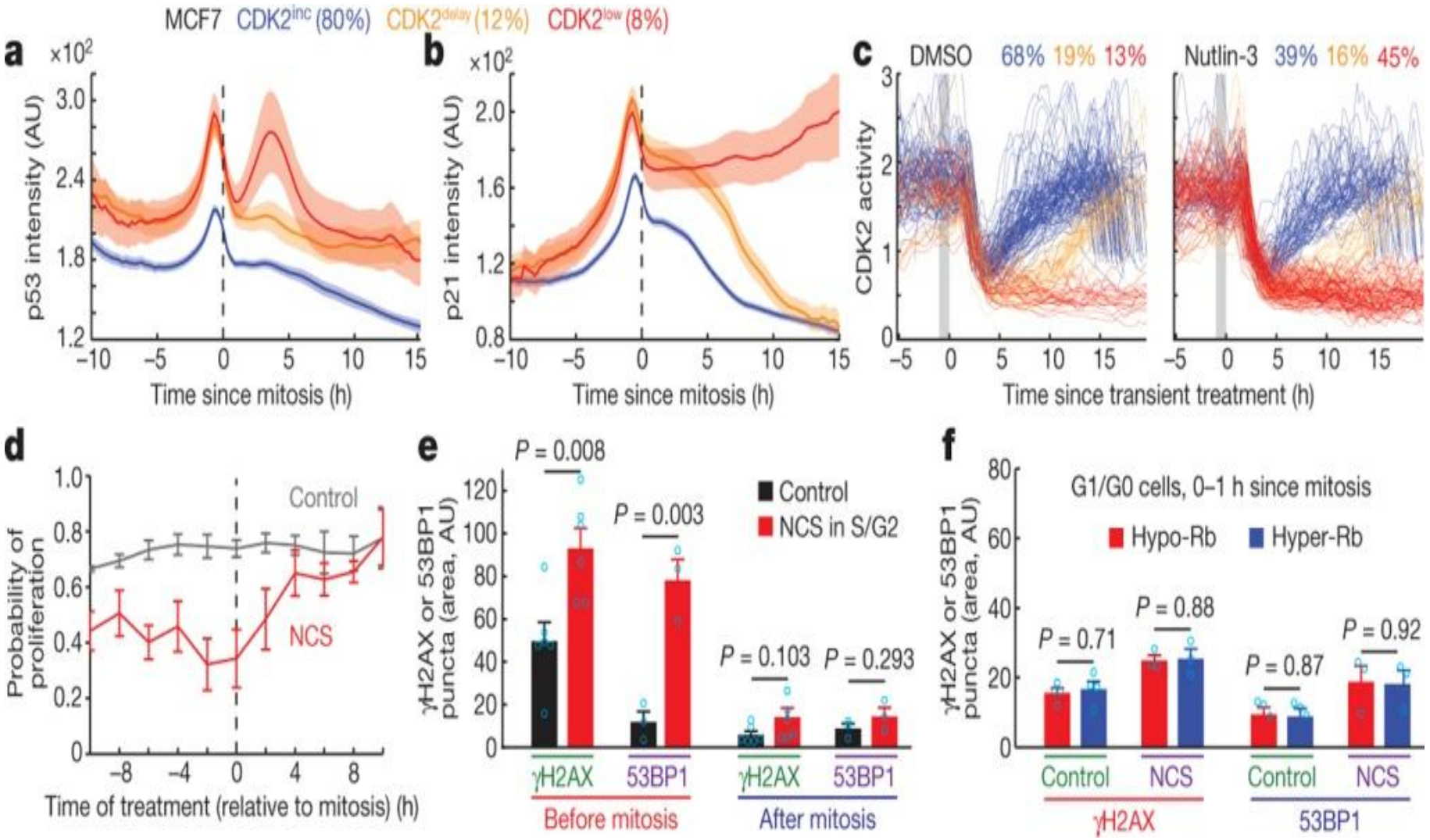

H W Yang *et al. Nature* 1–5 (2017) doi:10.1038/nature23880

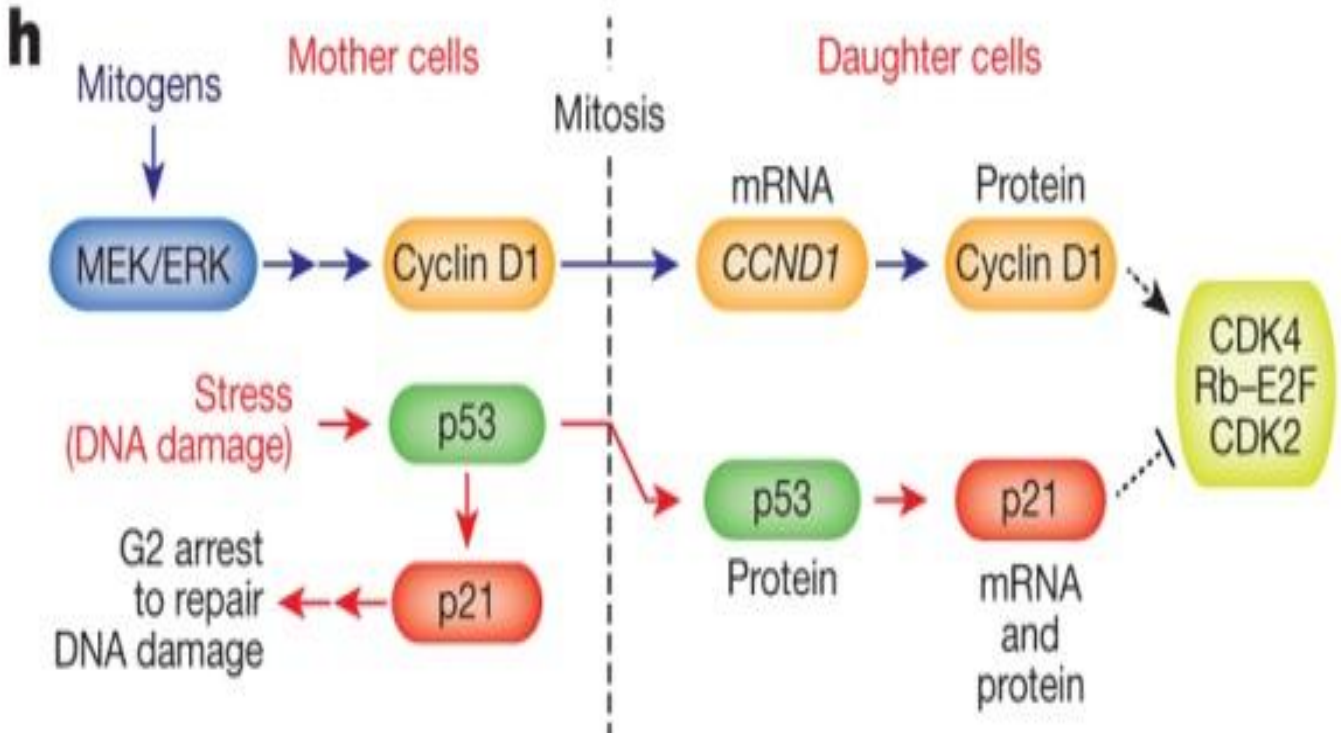
h
Mitogens
Mother cells
Mitosis
Daughter cells
mRNA
Protein
MEK/ERK
Cyclin D1
CCND1
Cyclin D1
CDK4
Rb–E2F
CDK2
Stress
(DNA damage)
p53
p53
p21
G2 arrest
to repair
DNA damage
p21
Protein
mRNA
and
protein

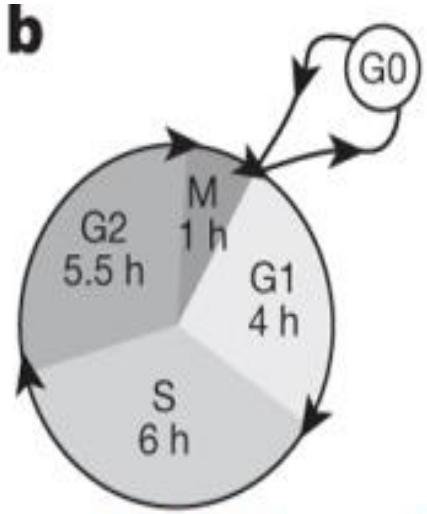
b
G0
M
1 h
G2
5.5 h
G1
4 h
S
6 h

) 2 to 4 h (4) 5

Акустические зеркала как сенсорные ловушки для летучих мышей

SENSORY TRAPS

Acoustic mirrors as sensory traps for bats

Stefan Greif,[1,2]*† Sándor Zsebők,[1]†‡ Daniela Schmieder,[1]§ Björn M. Siemers[1]

Sensory traps pose a considerable and often fatal risk for animals, leading them to misinterpret their environment. Bats predominantly rely on their echolocation system to forage, orientate, and navigate. We found that bats can mistake smooth, vertical surfaces as clear flight paths, repeatedly colliding with them, likely as a result of their acoustic mirror properties. The probability of collision is influenced by the number of echolocation calls and by the amount of time spent in front of the surface. The echolocation call analysis corroborates that bats perceive smooth, vertical surfaces as open flyways. Reporting on occurrences with different species in the wild, we argue that it is necessary to more closely monitor potentially dangerous locations with acoustic mirror properties (such as glass fronts) to assess the true frequency of fatalities around these sensory traps.

Anthropogenic changes to the environment, such as habitat alteration or interference with food resources, are often evidently detrimental to wild animals. Furthermore, ecologically novel cues are capable of misleading animals into responding maladaptively to formerly reliable environmental cues (*1*–*4*). Well-known examples are artificial light sources attracting insects and birds at night (*5*) or smooth human-made surfaces that aquatic insects mistake for bodies of water because of similar light polarization patterns (*6*). To find, evaluate, and mitigate such sensory traps requires consideration of the sensory ecology of a particular animal (*7*, *8*). The primary sensory modality for most bats is their echolocation system (*9*, *10*). Bats use the returning echoes of emitted calls to detect, classify, and localize objects in their environment (*11*–*13*).

In a previous study, we showed that bats perceive any extended, smooth, horizontal surface as a water body, resulting in drinking attempts. This is attributable to the acoustic mirror properties of smooth surfaces, which reflect calls away from the bat except for a strong perpendicular echo from below (*9*) (Fig. 1A). Several observations of bats colliding with smooth vertical surfaces (such as glass windows) suggest that bats have problems recognizing them (*14*–*16*). This raises concerns about the millions of artificial vertical smooth surfaces introduced in bat habitats and their hazard potential for injuries. We predicted that these collisions are based on the acoustic mirror paradigm and investigated the underlying sensory mechanism and possible occurrence in natural settings.

For our flight room experiments, we flew greater mouse-eared bats (*Myotis myotis*) in a continuous, rectangular flight tunnel (height 2.3 m, width 1.2 m) in the dark. A smooth metal plate (1.2 m × 2.0 m) was placed 1.2 m away from a corner of the felt-covered tunnel, either horizontally on the ground or vertically on the wall. The bats' flight behavior was recorded with two high-speed cameras (100 fps) and their echolocation calls with an ultrasound microphone (Fig. 1B) (*17*). Eleven bats were presented with the horizontal plate on the first night and the vertical plate on the second night. The order was reversed for 10 other bats. A trial lasted between 5 and 15 min with, on average, 20 passes by the plate. We counted drinking attempts as well as collisions with the plate, the ground, and the normal wall. Of 21 individuals, 19 collided with the vertical plate at least once (on average 22.8% of passes) but never with the horizontal plate (Wilcoxon matched-pair test, $P < 0.001$) nor any other parts of the wall. Thirteen individuals made at least one drinking attempt from the horizontal plate (on average 13.0% of passes), but none from the vertical plate (Wilcoxon matched-pair test, $P = 0.002$) (Fig. 2). After the experiments, all bats were carefully examined and no injuries were found.

To understand the sensory basis of those collisions with the vertical plate, we conducted analysis of the flight and echolocation behavior in the space immediately in front of the plate ("plate zone," limited by the plate's perpendicular projection; Fig. 1B) for 25 bats when flying toward the vertical plate. On the basis of our high-speed recordings, we categorized the approach events into three groups: (i) "near collision," where bats approached to within 25 cm of the plate (body-to-plate distance) but did not touch it; (ii) "collision with maneuver," where bats collided with the plate despite clear evasive maneuvers at the last moment; and (iii) "collision without maneuver," where bats collided without any noticeable evasive action. We measured the time and counted echolocation calls from entering the plate zone until reaching the closest point to the plate (either collision or turning point). We further calculated the bat's flight speed, the three-dimensional angle between its flight trajectory and the plate, and its distance to the plate when it entered the plate zone. The 78 events of approaching the plate (3.1 ± 1.8 events per individual, mean ± SD) consisted of 25 "near collision" events, 13 "collision with maneuver" events, and 40 "collision without maneuver" events (movie S1). We found that for "collision without maneuver" approaches, bats produced fewer calls, spent less time in front

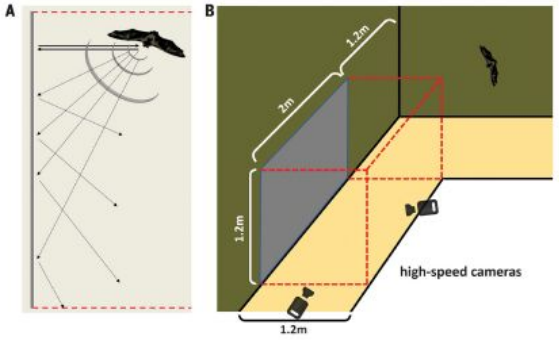

Fig. 1. Experimental setup. (**A**) Schematic of sound propagation at a smooth, vertical surface (top view). For a bat within the red-dashed "plate zone," sound impinging at an oblique angle is reflected away while only the perpendicularly impinging sound is reflected back. (**B**) Flight tunnel setup depicting the vertical situation. The smooth metal plate is shown in gray on the wall; the dashed lines represent the plate zone. In the horizontal situation, the smooth plate was lying on the floor of the plate zone (fig. S1).

[1]Sensory Ecology Group, Max Planck Institute for Ornithology, 82319 Seewiesen, Germany. [2]Department of Zoology, Tel Aviv University, Tel Aviv 6997801, Israel. *Corresponding author. Email: stefan.greif@gmail.com
†These authors contributed equally to this work.
‡Present address: Behaviour Ecology Research Group, Eötvös Loránd University, H-1117 Budapest, Hungary.
§Present address: Institute of Ecology and Evolution, University of Bern, 3012 Bern, Switzerland.

Группа исследователей из Германии и Швейцарии исследуют особенности эхолокации у летучих мышей.

Они пришли к выводу, что так называемое акустическое зеркало – гладкая и ровная поверхность – может быть для них сенсорной ловушкой и восприниматься ими как свободное пространство.

Митотическая транскрипция и волны реактивации генов при завершении митоза

Science

REPORTS

Cite as: K. C. Palozola *et al.*, *Science* 10.1126/science.aal4671 (2017).

Mitotic transcription and waves of gene reactivation during mitotic exit

Kathrine C. Palozola,[1,2] Greg Donahue,[2] Hong Liu,[2] Gregory R. Grant,[4] Justin S. Becker,[1,2] Allison Cote,[2] Hongtao Yu,[6] Arjun Raj,[2] Kenneth S. Zaret[1,2]*

[1]Institute for Regenerative Medicine, Perelman School of Medicine, University of Pennsylvania, Philadelphia, PA 19104-5157, USA. [2]Department of Cell and Developmental Biology, Perelman School of Medicine, University of Pennsylvania, Philadelphia PA, 19104-5157, USA. [3]Department of Biochemistry and Molecular Biology and Tulane Center for Aging, Tulane University Health Sciences Center, New Orleans, LA 70112, USA. [4]The Institute for Translational Medicine and Therapeutics, Department of Genetics, Perelman School of Medicine, University of Pennsylvania, Philadelphia, PA 19104, USA. [5]Department of Bioengineering, University of Pennsylvania, Philadelphia, PA 19104, USA. [6]Howard Hughes Medical Institute, Department of Pharmacology, University of Texas Southwestern Medical Center, Dallas, TX 75390, USA.

*Corresponding author. Email: zaret@upenn.edu

Although the genome is generally thought to be transcriptionally silent during mitosis, technical limitations have prevented sensitive mapping of transcription during mitosis and mitotic exit. Thus, the means by which the interphase expression pattern is transduced to daughter cells have been unclear. We used 5-ethynyluridine to pulse-label transcripts during mitosis and mitotic exit and find that many genes exhibit transcription during mitosis, as confirmed by FITC-UTP labeling, RNA FISH, and RT-qPCR. The first round of transcription immediately following mitosis primarily activates genes involved in the growth and rebuilding of daughter cells, rather than cell type-specific functions. We propose that the cell's transcription pattern is largely retained at a low level through mitosis, whereas the amplitude of transcription observed in interphase is re-established during mitotic exit.

During mitosis, chromatin condenses (*1*), gene regulatory machinery is largely evicted from chromatin (*2*–*4*), and transcription is thought to be silenced (*5*–*7*). Yet reactivation of a specific gene expression program is needed to maintain cell identity during exit from mitosis. Long-distance interactions across the genome are lost during mitosis (*8*), as is hypersensitivity at distal enhancers, but not at promoters (*9*). "Bookmarking" transcription factors remain bound in mitosis to a subset of their interphase sites (*10*–*15*). Knock-down of these factors during mitosis delays reactivation of target genes (*10*, *11*, *13*), though the proper transcriptome is eventually regenerated. Thus the basis for identity maintenance during mitosis remains unclear, and the hierarchy by which genes are reactivated during mitotic exit is not understood.

Because of nuclear envelope breakdown in mitosis and hence the inability to isolate nuclei for direct labeling of transcripts (*16*), genome-wide studies during mitotic exit used RNA Polymerase II (RNAP2) cross-linking to assess active transcription (*4*, *17*) and found a burst in RNAP2 binding to promoters approximately 60-90 min after release from mitotic arrest (*17*). However, the dynamic range of antibody-based methods is much less than from direct measurements of nascent transcription and crosslinking artifactually causes protein exclusion from mitotic chromatin (*14*, *18*). Transcription elongation inhibition of prometaphase HeLa cells elicits paused RNAP2 at promoters, suggesting the presence of elongating enzyme, even though elongating RNAP2 was not detected directly (*19*). The study also mapped non-polyadenylated, chromatin-associated RNAs from prometaphase cells, but it was unclear whether these RNAs were transcribed during mitosis or, as suggested by the authors, at the G2/M transition. A study of pulse-labeled transcripts in arrested MCF-7 human breast cancer cells used nuclear isolation for BrUTP labeling and hence did not appear to be assessing mitotic cells (*20*).

To define the timing of transcription events during mitotic exit, we used the cell-permeable 5-ethynyluridine (EU) to pulse-label nascent transcripts (*21*) in intact HUH7 human hepatoma cells during nocodazole-induced mitotic arrest, mitotic exit, and in asynchronous cells. Importantly, arrested cells, enriched by mitotic shake-off, were highly pure (fig. S1, A to D) and re-enter G1 (fig. S1, E to K). Previously, we labeled transcripts with EU during mitotic exit in HUH7 cells and attached azide-fluorophore, discovering that bulk global transcription initiates approximately 80' after nocodazole washout (*11*). Based on this assessment of global reactivation, here we pulse-labeled transcripts at 0, 40, 80, 105, 165, and 300 min after nocodazole wash-out in HUH7 cells, but instead conjugated azide-biotin to the EU-RNA to measure the relative changes between over time (Fig. 1A). The addition of biotin allowed us to use streptavidin beads to isolate EU-

Группа американских учёных исследовала транскрипцию генов время митоза.

Несмотря на то, что при митозе хромосомы находятся в конденсированном состоянии, транскрипция некоторых генов хоть и очень слабая, но идёт, что и удалось показать с помощью гибридизации РНК и ПЦР в реальном времени

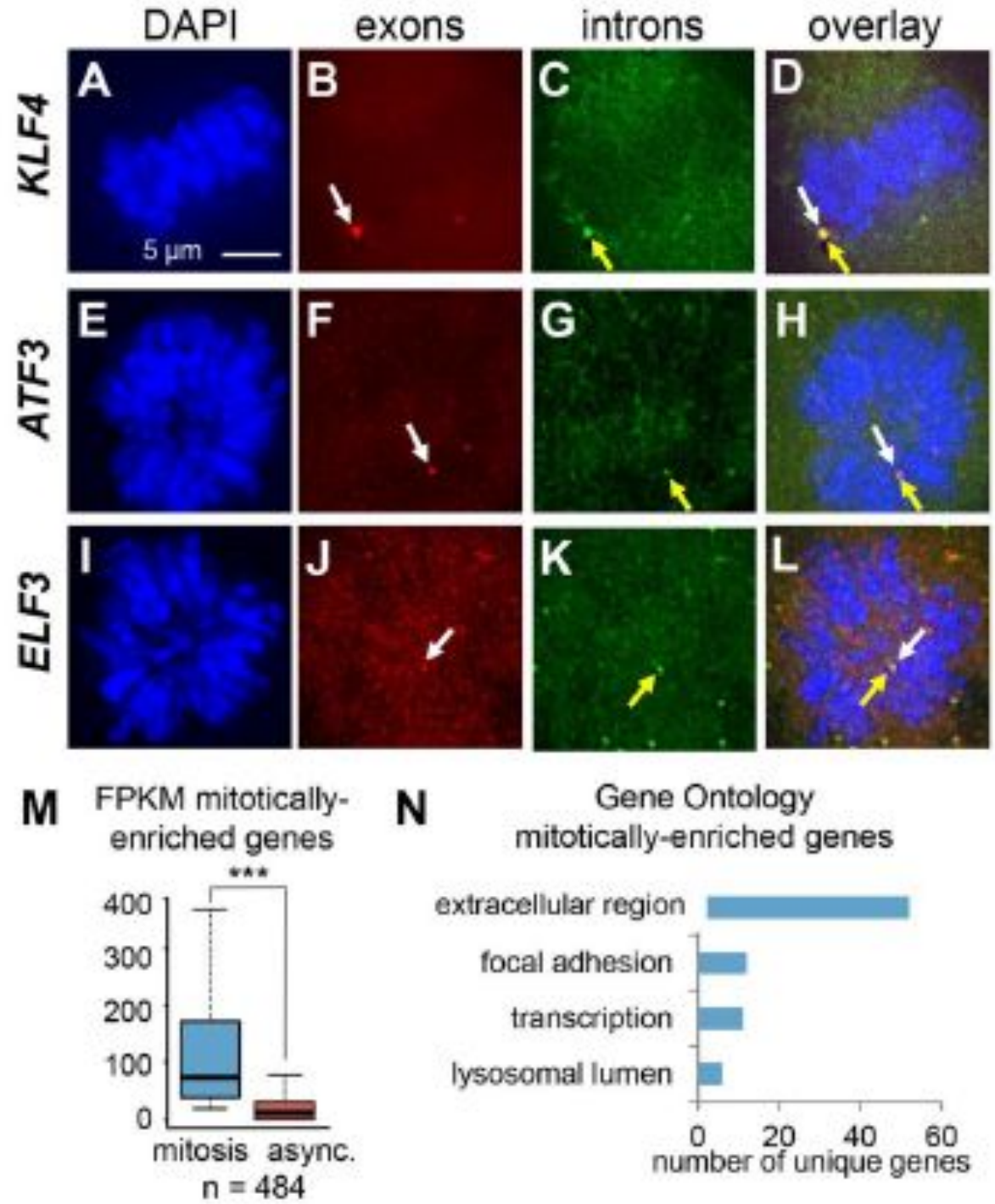
DAPI
exons
introns
overlay
KLF4
ATF3
ELF3
A
B
C
D
E
F
G
H
I
J
K
L
5 µm
M
FPKM mitotically-enriched genes
***
400
300
200
100
0
mitosis
async.
n = 484
N
Gene Ontology mitotically-enriched genes
extracellular region
focal adhesion
transcription
lysosomal lumen
0
20
40
60
number of unique genes

Усовершенствованная сверка регулирует точность таргетирования CRISPR-cas9

Enhanced proofreading governs CRISPR–Cas9 targeting accuracy

Janice S. Chen, Yavuz S. Dagdas, Benjamin P. Kleinstiver, Moira M. Welch, Alexander A. Sousa, Lucas B. Harrington, Samuel H. Sternberg, J. Keith Joung, Ahmet Yildiz & Jennifer A. Doudna

Affiliations | Corresponding author

Nature (2017) | doi:10.1038/nature24268

Received 28 June 2017 | Accepted 12 September 2017 | Published online 20 September 2017

PDF | Citation | Article metrics

Abstract

Abstract • Main • Author information • Supplementary information

The RNA-guided CRISPR–Cas9 nuclease from *Streptococcus pyogenes* (SpCas9) has been widely repurposed for genome editing [1–4]. High-fidelity (SpCas9-HF1) and enhanced specificity (eSpCas9(1.1)) variants exhibit substantially reduced off-target cleavage in human cells, but the mechanism of target discrimination and the potential to further improve fidelity are unknown [5–9].

И снова она! Американские учёные с помощью Ферстеровского резонансного переноса выяснили особенности работы системы CRISPR-cas9 когда она в редких случаях ошибается.

Кроме того, был создан более точный вариант системы HypaCas9

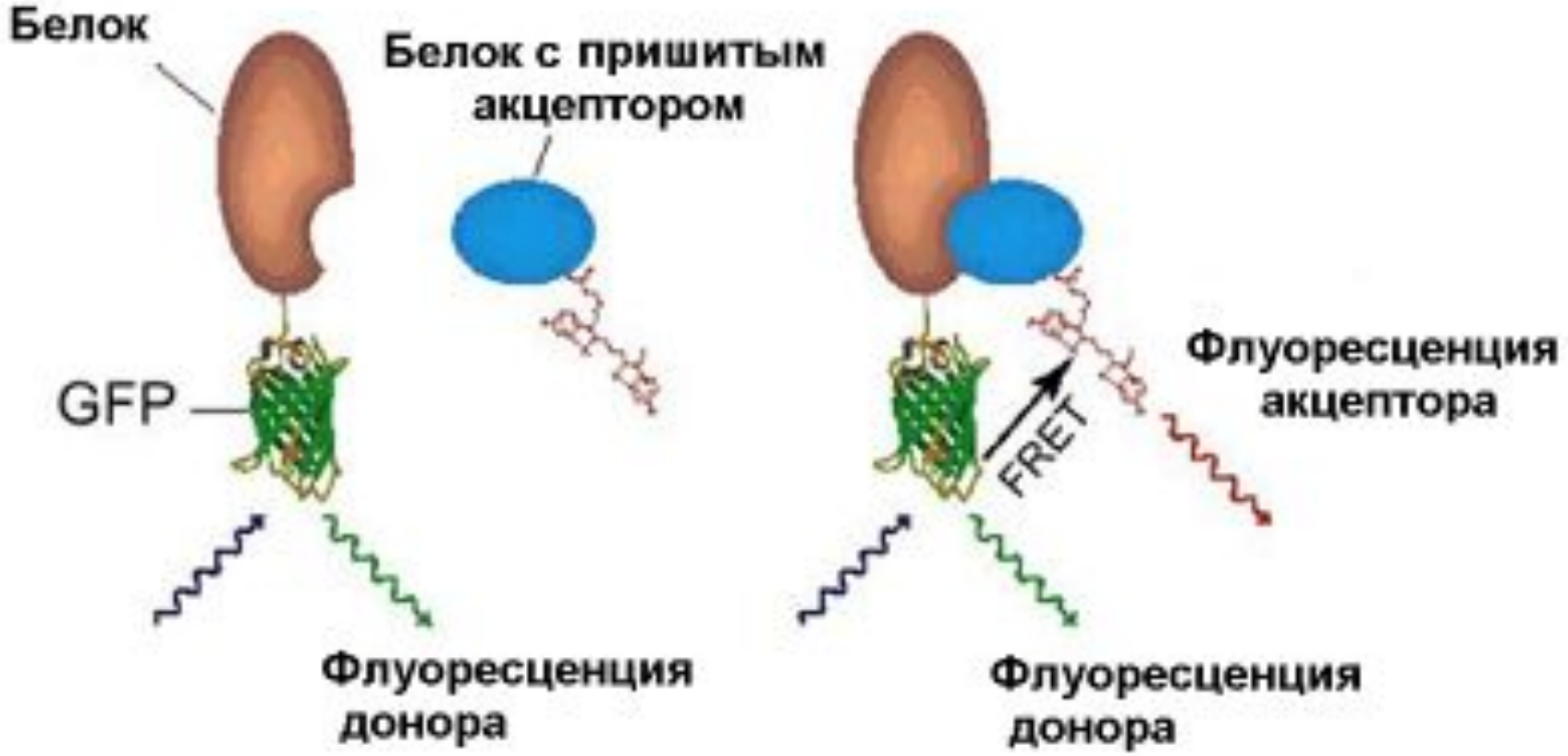

Wouters et al.- Trends in Cell Biol., 2001

Временные механизмы сосуществования способствуют широтному градиенту разнообразия лесов

LETTER

doi:10.1038/nature24038

Temporal coexistence mechanisms contribute to the latitudinal gradient in forest diversity

Jacob Usinowicz[1], Chia-Hao Chang-Yang[2], Yu-Yun Chen[2], James S. Clark[3], Christine Fletcher[4], Nancy C. Garwood[5], Zhanqing Hao[6], Jill Johnstone[7], Yiching Lin[8], Margaret R. Metz[9], Takashi Masaki[10], Tohru Nakashizuka[11,12], I-Fang Sun[2], Renato Valencia[13], Yunyun Wang[6], Jess K. Zimmerman[14], Anthony R. Ives[1] & S. Joseph Wright[14,15]

The tropical forests of Borneo and Amazonia may each contain more tree species diversity in half a square kilometre than do all the temperate forests of Europe, North America, and Asia combined[1]. Biologists have long been fascinated by this disparity, using it to investigate potential drivers of biodiversity[2]. Latitudinal variation in many of these drivers is expected to create geographic differences in ecological[2–4] and evolutionary processes[4,5], and evidence increasingly shows that tropical ecosystems have higher rates of diversification, clade origination, and clade dispersal[5,6]. However, there is currently no evidence to link gradients in ecological processes within communities at a local scale directly to the geographic gradient in biodiversity. Here, we show geographic variation in the storage effect, an ecological mechanism that reduces the potential for competitive exclusion more strongly in the tropics than it does in temperate and boreal zones, decreasing the ratio of interspecific-to-intraspecific competition by 0.25% for each degree of latitude that an ecosystem is located closer to the Equator. Additionally, we find evidence that latitudinal variation in climate underpins these differences; longer growing seasons in the tropics reduce constraints on the seasonal timing of reproduction, permitting lower recruitment synchrony between species and thereby enhancing niche partitioning through the storage effect. Our results demonstrate that the strength of the storage effect, and therefore its impact on diversity within communities, varies latitudinally in association with climate. This finding highlights the importance of biotic interactions in shaping geographic diversity patterns, and emphasizes the need to understand the mechanisms underpinning ecological processes in greater detail than has previously been appreciated.

Tree species diversity at the hectare scale increases by an order of magnitude from boreal to temperate forests, and again from temperate to tropical forests, despite the fact that basic resources, such as soil nutrients and sunlight, act similarly in their role as limiting resources across latitudes[1]. Even with higher speciation rates, maintaining these high levels of tropical diversity over geological time scales is likely to require coexistence mechanisms that can reduce the potential for extinction as a result of competitive exclusion between species[7]. Numerous processes have been identified in tropical forests that could prevent competitive exclusion and allow a high degree of coexistence[8], including selective predation by specialist herbivores and pathogens[9–11], resource competition[12], trade-offs between competitive and colonization abilities[13–15], adoption of different adult growth forms[16], and species-specific responses to variation among germination sites[17]. Ecological coexistence theory states that any of these mechanisms could promote coexistence by making interspecific competition consistently weaker than intraspecific competition[18]. However, these coexistence conditions are rarely quantified, and there is little evidence that any of these processes vary in strength across latitudes in a manner consistent with geographic biodiversity patterns[19–21].

Here, we investigate geographic variation in potential coexistence, resulting from reduced interspecific synchrony of tree recruitment. Reducing synchrony among recruitment periods can lead to interactions with conspecific individuals clustering in periods favourable for reproduction; if adults are sufficiently long-lived to buffer populations through unfavourable periods, this can ultimately decrease interspecific competition relative to intraspecific competition through the storage effect[18]. For tree communities, inter-annual variation in recruitment into the understory contributes to the concentration of intraspecific, relative to interspecific, seedling interactions[1,22]. Crucially, interspecific annual asynchrony derives from species-specific responses to environmental fluctuations over the course of the year, during reproduction, germination, and post-germination periods[23]. The seasonal timing of reproduction is important because it determines the conditions to which species are exposed during germination and post-germination processes[23,24].

Annual climate variation is a major driver of inter-annual fluctuations in both biotic and abiotic conditions, but is often not distributed evenly throughout the year. This is a well-established relationship in tropical forests for which El Niño and La Niña events are the major source of inter-annual variation; these events hit more strongly in particular months (for example, El Niño can exacerbate dry conditions in the January–April dry season of many Caribbean forests) and therefore have larger effects on the seed production of species that reproduce at these times[23,24]. As a consequence, species reproducing at different times in a season will experience different amounts of variation in their recruitment in a given year; reduced seasonal synchrony may reduce inter-annual synchrony by increasing the likelihood that species experience climate conditions differently in the same year. Following on from this hypothesis, the longer and more stable growing seasons in the tropics should permit greater differentiation between species in the seasonal timing of their reproduction[5], and therefore a latitudinal gradient in the storage effect should emerge as a result of an underlying gradient in seasonality[25,26].

We hypothesized that the storage effect promotes coexistence more strongly in tropical forests than in temperate or boreal forests (premise 1), because longer growing seasons at lower latitudes correspond to a reduction in between-year synchrony in species' reproduction (premise 2), and tested these two premises separately. We assembled

[1]Department of Integrative Biology, University of Wisconsin, Madison, Wisconsin, USA. [2]Department of Natural Resources and Environmental Studies, National Dong Hwa University, Hualien, Taiwan. [3]Nicholas School of the Environment, Duke University, Durham, North Carolina, USA. [4]Forest Research Institute Malaysia, Kuala Lumpur, Malaysia. [5]Department of Plant Biology, Southern Illinois University, Carbondale, Illinois, USA. [6]Institute of CAS Key Laboratory of Forest Ecology and Management, Institute of Applied Ecology, Chinese Academy of Sciences, Shenyang, China. [7]Institute of Arctic Biology, University of Alaska Fairbanks, Fairbanks, Alaska, USA. [8]Department of Life Science, Tunghai University, Taichung, Taiwan. [9]Biology Department, Lewis & Clark College, Portland, Oregon, USA. [10]Forestry and Forest Products Research Institute, Tsukuba, Ibaraki, Japan. [11]Graduate School of Life Sciences, Tohoku University, Sendai, Miyagi, Japan. [12]Research Institute for Humanity and Nature, Kyoto, Japan. [13]Laboratorio de Ecología de Plantas, Herbario QCA, Pontificia Universidad Católica del Ecuador, Quito, Ecuador. [14]Department of Environmental Science, University of Puerto Rico at Río Piedras, San Juan, Puerto Rico. [15]Smithsonian Tropical Research Institute, Apartado 0843-03092, Balboa, Panama.

Исследователи из Китая, Тайваня и США изучали механизмы формирования широтного градиента биоразнообразия лесов.

Предполагается, что климатические различия между лесами экватора и лесами севернее и южнее его способствуют ослаблению конкурентного исключения – организмы легче находят субниши в пределах общих экологических ниш.